Pharmaceutical Research, Vol. 27, No. 4, April 2010 (© 2010)
DOI: 10.1007/s11095-010-0066-1

Research Paper

Measurement and Modeling of Diffusion Kinetics of a Lipophilic Molecule Across Rabbit Cornea

Chhavi Gupta,[1] Anuj Chauhan,[1] Raj Mutharasan,[2] and Sangly P. Srinivas[3,4]

Received November 23, 2009; accepted January 8, 2010; published online February 25, 2010

Purpose. To develop a kinetic model for representing the diffusion and partitioning of Rhodamine B (RhB), a fluorescent lipophilic molecule, across the cornea for gaining insights into pharmacokinetics of topical drugs to the eye.
Methods. Rabbit corneas mounted underneath a custom-built scanning microfluorometer were perfused with Ringers on both sides of the tissue. After a step change in RhB on the tear side, transients of trans-corneal fluorescence of RhB were measured at a depth resolution ~ 8 μm.
Results. RhB distribution exhibited discontinuities at the interface between epithelium and stroma, and between stroma and endothelium. In each of the layers, fluorescence was non-uniform. Fluorescence was elevated in the epithelium and endothelium relative to the stroma. Modeling of RhB transport by diffusion in each layer and stipulation of partitioning of RhB at the cellular interfaces were required to account for trans-corneal penetration kinetics of RhB. The model parameters, estimated using the unsteady state trans-corneal RhB profiles, were found to be sensitive, and the model predicted the experimental profiles accurately.
Conclusions. Conventional pharmacokinetic models that depict cornea as a single compartment do not predict the depth-dependent kinetics of RhB penetration. The proposed model incorporates realistic transport mechanisms and thereby highlights the influence of physicochemical properties of drugs on trans-corneal kinetics.

KEY WORDS: Cornea; Confocal microfluorometer; Diffusion; Lipophilicity; Lipophilic molecule; Partition coefficient; Rhodamine B; Topical pharmacokinetics.

INTRODUCTION

Drug delivery to the anterior segment of the eye is achieved chiefly by topical administration (1,2). More than 90% of the drugs instilled are lost by tear drainage from the ocular surface, and only a small fraction gets absorbed across the cornea, sclera, and/or conjunctiva. The rate of tear drainage is determined by the blink action, which pumps the tears from the ocular surface into the nasolacrimal duct. Consequently, the topically applied drug is absorbed across the nasal mucosa into systemic circulation. This fraction of the applied drug, along with the drug absorbed across the conjunctival epithelium, may provoke systemic adverse effects. Thus, topical administration, besides having the potential for systemic toxicity, results in a rapid decay of the drug concentration on the ocular surface (1-5). Since the half-life of the drug on the ocular surface is only 4–6 min (1,4,6,7) and because of potential for systemic toxicity, there is a need for rational design of topical drugs such that kinetics of their penetration into the intraocular structures of the eye is optimized.

As noted above, most topical drugs access the intraocular structures by penetration across the cornea. Trans-scleral penetration is known to play a role only for a few drugs (1,2,4,5). In order to represent the kinetics of drug penetration across the cornea, it is important to consider heterogeneity of the tissue across its depth. Briefly, the cornea is a transparent structure with a central matrix of connective tissue called the stroma bounded by cellular layers. The anterior cellular layer is the epithelium. This layer is stratified into ~5-6 layers and is ~40 μm thick in humans. The superficial epithelium forms the main barrier to the penetration of topically applied hydrophilic drugs as it exhibits multi-stranded tight junctions (8).

It is well known that lipophilic drugs penetrate the epithelium readily, presumably by dissolving in the lipid bilayers of the plasma membrane and subsequent movement by the transcellular route. For subsequent transport toward the anterior chamber, however, the ability of the drug to partition into the stroma is an important consideration. In fact, the stroma, being hydrophilic with >80% water, offers no more resistance than an equivalent thickness of water layer for most topical drugs (9). Thus, although the drugs may

[1] Department of Chemical Engineering, University of Florida, Gainesville, Florida, USA.
[2] Department of Chemical and Biological Engineering, Drexel University, Philadelphia, Pennsylvania 19104, USA.
[3] School of Optometry, Indiana University, 800 East Atwater Avenue, Bloomington, Indiana 47405, USA.
[4] To whom correspondence should be addressed. (e-mail: srinivas@indiana.edu)

diffuse readily in the stroma, poor partitioning of lipophilic drugs into it would be a major determinant for transport across the cornea. Finally, the posterior layer of the cornea is a monolayer of leaky endothelium, and thus does not offer much resistance to the paracellular movement of solutes. This multi-laminate structure (i.e., *oil:water:oil* layers) of the cornea, shown schematically in Fig. 1, strongly suggests the importance of including partitioning of the drug into various layers in describing for its trans-corneal penetration.

Pharmacokinetics of topical drugs to the eye has been frequently described by compartmental models (10-13), which assume that drug concentration becomes uniform throughout the cornea instantaneously after topical administration. Hence, the compartmental models disregard the heterogeneity (i.e., multi-laminate structure) of the cornea and diffusive nature of transport in each of its layers as described above. The over-simplification has led to a poor understanding of the dynamics of trans-corneal drug transport and consequently to empirical approaches for design of dosage regimen and design of topical drugs. Several attempts have been made to model the transport across the cornea, taking its multi-laminate structure into consideration (14-16). In the absence of measurements of trans-corneal concentration profiles, the distributed parameter models developed to date are based only on theoretical. Assumptions used in such models have never been tested for robustness of the resulting models. In essence, it is difficult to determine which transport step among those involved in the drug penetration forms a key determinant of rate of penetration.

We envisage in this study, the overall trans-corneal penetration of drug can be broken down into several serial and parallel elementary steps consisting of drug-cell binding/partition dynamics, interfacial resistance to transport, and/or transport dynamics inside the cells. Since measurement of concentration *vs*. depth profiles of real drug molecules is not easily achieved, in this study, we have employed a fluorescent dye Rhodamine B (RhB) as a model lipophilic drug analog (17), and determined its concentration profile across the cornea by a custom-built confocal fluorescence microscope. The transient concentration profiles were used subsequently in developing a phenomenological diffusive transport model. Thus, for the first time, the model reported herein exemplifies a microscopic approach to correlate the physico-chemical properties of drug analogs to their transport properties across the cornea.

MATERIALS AND METHODS

Rhodamine B (RhB; Cat #R6626; MW: 479; CAS Number 81-88-9) and all other reagents for Ringers solution were obtained from Sigma Chemical Company (St. Louis, MO). Eyes were obtained from freshly killed albino (New Zealand White) rabbits of either sex. All procedures for animal handling were in accordance with the guidelines set by the Association for Research in Vision and Ophthalmology (ARVO) and approved by Laboratory Animal Care Committee of Stanford University. Experiments were performed in the laboratory of (late) Prof. David Maurice, Ophthalmology at Stanford University, by one of the authors (S.P. Srinivas).

The corneas were isolated and mounted as previously described (18,19). They were maintained at 34°C and perfused with HCO_3^- Ringers (containing reduced glutathione, glucose, adenosine, 40 mM HEPES, and 40 mM $NaHCO_3$) at the posterior endothelial surface (~2-3 μL/min)

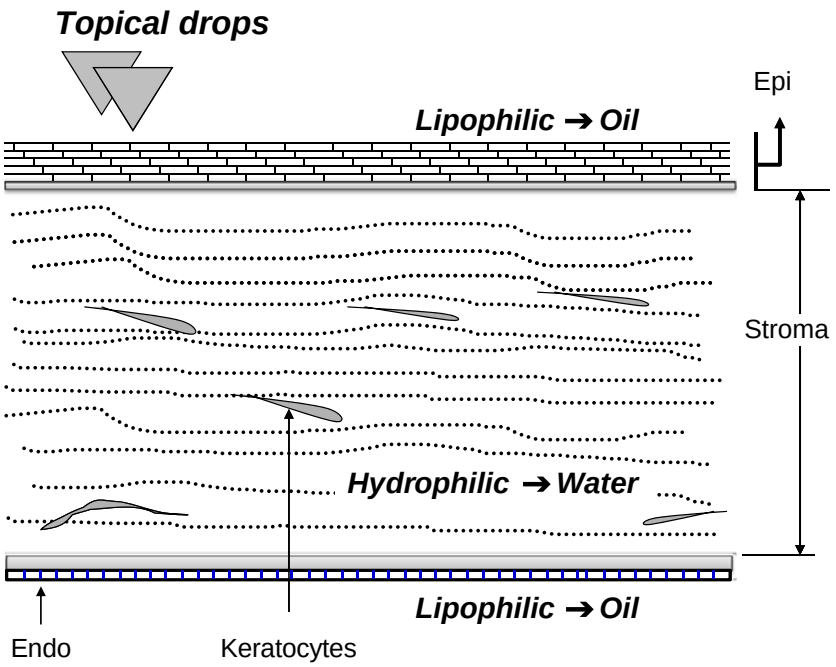

Fig. 1. Cornea as a *Oil:Water:Oil* multi-laminate. This is a widely accepted pharmacokinetic view of the cornea. However, most pharmacokinetic models to date assume either the whole cornea as a single compartment or three well-stirred compartments. The innovation of the model in this study assumes the three layers of the cornea to be uniform and their transport across each layer to occur by diffusion.

(20). The epithelial surface was exposed to Ringers solution of same molality except that it contained RhB when needed and was replaced every 30 min. The volume of the receiver chamber was 300 μL, while the donor side volume exceeded 0.5 mL.

The trans-corneal profiles of RhB were obtained using a custom-built confocal scanning microfluorometer, as described previously (18,19). Depth scanning was performed through a stepper motor coupled mechanically to the fine focus knob of the microscope. Depth resolution was ~8 μm at a sensitivity of 10^{-6} gm/mL of fluorescein (signal-to-noise ratio > 20) using a 40× water immersion objective of 0.75 NA (Zeiss Inc) (19,21). Scanning was performed at ~600 μm/min over 800 μm depth. RhB fluorescence was excited at 530± 10 nm using an interference filter and emission was collected >580 nm with a long pass filter. The light source was a 10 W Halogen lamp, and the intensity of light used for excitation did not cause any noticeable photobleaching. About 30 min after mounting the cornea, the epithelial surface was exposed to RhB dissolved (1 μg/mL) in the Ringers. Scatter and fluorescence scans were measured to obtain corneal thickness and trans-corneal concentration profile of RhB, respectively. After exposure to RhB, the trans-corneal scans were carried out for 3-4 h. More than six experiments were performed, and the data from one typical experiment has been considered in this study for analysis. The experimental data alone were previously presented in an abstract form by Srinivas and Maurice at the Association of Research in Vision and Ophthalmology (22).

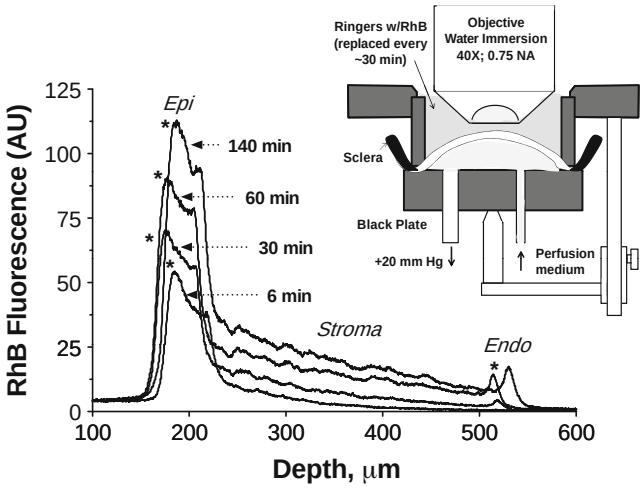

Fig. 2. Trans-corneal penetration of RhB across rabbit cornea mounted *in vitro*. RhB was held at a constant concentration by periodic replacement of the solution containing the dye on the tear-side (donor chamber; ~0.5 mL; every 30 min). Y-axis represents fluorescence in arbitrary units (AU). The fluorescence scans were performed with a custom-built scanning microfluorometer (see Methods) with a depth resolution of ~8 μm using a 40x objective (Zeiss, Inc. 0.75 NA; water immersion). Inset shows schematic of the experimental set-up used for mounting the cornea and the trans-corneal scanning microfluorometer arrangement. The receiver chamber, which was ~300 μL, was perfused continuously with HCO_3^- Ringers at a rate of ~3 μL/min.

RESULTS

Penetration of Rhodamine B Across the Cornea

The implications of the multi-layer oil:water:oil structure of cornea, as well as the shortcomings of the compartmental models, are illustrated by our experimental observations of the penetration of RhB, as shown in Fig. 2. The inset in Fig. 2 shows a schematic of the experimental perfusion set-up employed for the experiments.

It is evident from the fluorescence profiles that RhB distributes across the cornea with distinct discontinuities at the cellular boundaries between epithelium and stroma as well as between stroma and endothelium. Furthermore, the fluorescence is non-uniform in the epithelial and stromal layers. Also noteworthy is that the fluorescence is elevated in the lipophilic cellular layers (epithelium and endothelium) relative to its level in the hydrophilic stroma. This indicates partitioning of RhB into the lipophilic structures across the cornea. The time- and position-dependent fluorescence gradients, apparent in the epithelium and stroma, represent diffusional resistance for RhB transport. These observations, in turn, suggest that RhB in epithelium and stroma are not of uniform concentration and they cannot be construed as homogenous compartments, let alone the entire cornea. Therefore, penetration of RhB cannot be described by conventional compartmental models. Furthermore, the fluorescence profiles of RhB in Fig. 2 also indicate that fluorescence of RhB at the epithelial surface reaches a high value within 6 min and then continues increasing. Similarly, the fluorescence peak is also observable at the endothelium after 30 min, and the peak height increases slowly. These findings suggest accumulation of RhB in the epithelium and endothelium with almost negligible accumulation in the stroma.

Model for Penetration Kinetics of Rhodamine B

In this section, we develop a general model for trans-corneal penetration of a lipophilic solute which includes the experimental observations made above with RhB. The model parameters will be estimated using unsteady state trans-corneal RhB profiles experimental shown in Fig. 2. We assume that RhB is not metabolized in accordance with the physio-chemical properties of RhB during its transport across the cornea.

Transport Across the Cellular Layers

A general model for solute transport in the cornea can be constructed at various length scales. A simplest model is one in which cornea is assumed to be a single, well-stirred compartment. This can be further simplified by requiring the multilayer structure of the cornea, while still treating each layer as homogeneous with characteristic diffusivity and partition coefficients. Further improvement is possible by incorporating the cellular structures in each of the layers and including heterogeneities in each layer/cells. But the degree of refinement in the model is dictated by the resolution of the experimental data that is needed to estimate the model parameters. The experimental data described above has a spatial resolution of ~8 μm, and hence the appropriate model is one that treats each layer as a homogeneous tissue.

However, as explained below, the slow accumulation of RhB in the cornea could potentially arise from mechanisms that operate at the cellular level. Since the model must account for the slow accumulation, we propose a further refinement in which a shorter length scale is added into the model at the longer length scale (i.e., one involving homogenous individual layers) discussed above. Out of necessity, transport at the cellular level is neglected, since the experimental data do not permit identification of parameters associated with such phenomena.

The first step in the trans-corneal penetration of a lipophilic solute from the tear side is its partitioning into the lipid bilayers of the plasma membrane of the superficial corneal epithelium that is in contact with the tears. Depending on the octanol-water partition coefficient, a fraction of the solute in the epithelial bilayer will partition into the hydrophilic cytoplasm. Once in the cytoplasm, the solute may partition into putative intracellular lipophilic domains, such as the lipid membranes of the intracellular organelles (e.g., endoplasmic reticulum) (Fig. 3). The partitioning behavior may be complex, but is treated as reversible, non-saturable linear binding as an approximation in the current analysis. We model the transport steps described above as follows.

The rate of transport from the epithelial bilayer to the intracellular domains is expressed as the product of a rate constant (denoted by k_1) and a net driving force for transport given by $\left(C_1 - \frac{C_1^b}{K_1}\right)$, where C_1 is the average concentration of the solute in the epithelial bilayer, C_1^b is the average concentration in the intracellular lipophilic domains, and K_1 is the ratio of C_1^b and C_1 at equilibrium. More precisely, C_1 is the concentration in the lipid bilayers based on total cell volume; i.e., it is the product of the actual concentration in the bilayers and the volume fraction of the bilayers in the epithelial cells. Similarly, $C_1{}^b$ is the product of the concentration in the internal hydrophobic regions and the volume fraction of such regions in the cell. The rate constant, k_1, may also be considered as the permeability of cytoplasm that separates the epithelial bilayer from intracellular lipophilic domains.

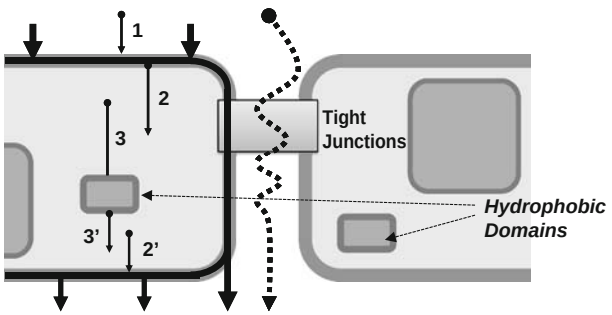

Fig. 3. Transport across the cellular layers: The main mechanism for transport of lipophilic solutes is through the lipid bilayers of the plasma membrane (dark arrow). Another important but slower mechanism leads to continued accumulation of hydrophobic solute in the intracellular hydrophobic domains (e.g., membrane associated with endoplasmic reticulum). This mechanism can be resolved into following steps in sequence: (1) transport by partition into the bilayer of the plasma membrane from tears, (2) partitioning of the drug into cytoplasm from the bilayer, and (3) partitioning into intracellular hydrophobic domains. Hydrophilic solutes can pass through paracellular pathways independently of their partition coefficient and degree of ionization (dotted arrow). Steps 2' and 3' represent steps analogous to the required 2 and 3, which permit an alternative route for trans-cellular movement of the lipophilic solutes.

Based on the above model for accumulation in the intracellular domains, transient mass balance of the solute in the corneal epithelium and its association with the intracellular lipophilic domains can be written as

$$\frac{\partial C_1}{\partial t} = D_1 \frac{\partial^2 C_1}{\partial y^2} - k_1\left(C_1 - \frac{C_1^b}{K_1}\right)$$
$$\frac{\partial C_1^b}{\partial t} = k_1\left(C_1 - \frac{C_1^b}{K_1}\right) \quad (1)$$

In the above and subsequent equations, the y-coordinate refers to the depth across the cornea, y=0 is at the tear-epithelium, and interface and t refers to time (Fig. 4). The parameter D_1 is the effective diffusion coefficient in the lipid bilayer. For ease of reference, we have compiled all the parameters of the model in Table I.

In the mass balance for the free RhB, the first term on the right side of Eq. 1 represents the diffusion of the solute through the lipid bilayers, which is the dominant transport mechanism. However, this cannot capture the slow accumulation of RhB in the cornea, as observed in Fig. 2. To account for the slow accumulation, the second term is added on the right side of Eq. 1. As explained above, we assume that this second term could be the contribution from the transport at the cellular level of the solute from the lipid bilayers to internal organelles across the cytoplasm. We also note that the second term on the right side of the mass balance can also be interpreted as a first-order, reversible binding of the solute, which could also lead to the slow accumulation of the solute. Since the expression for the rate-limiting binding is mathematically identical to that for diffusion-limited rates of transport into the internal hydrophobic domains, we combine the two rate mechanisms together. Both slow binding and transport through the cytoplasm to internal organelles can lead to slow accumulation, and so further experiments with high spatial resolution or with single cells are required to determine the correct mechanism.

Since the posterior surface of the cornea is also a cellular layer, we assume that the model for transport across the endothelium is mathematically similar to the epithelium. Thus, the trans-endothelial solute transport is described as

$$\frac{\partial C_3}{\partial t} = D_3 \frac{\partial^2 C_3}{\partial y^2} - k_3\left(C_3 - \frac{C_3^b}{K_3}\right)$$
$$\frac{\partial C_3^b}{\partial t} = k_3\left(C_3 - \frac{C_3^b}{K_3}\right) \quad (2)$$

In the above subscript 3 refers to endothelium. Thus, the parameters D_3, K_3, k_3, C_3, and $C_3{}^b$ have the same definitions as the corresponding parameters noted for the epithelium (Table I).

Transport Across the Stroma

The corneal stroma is composed of ~300 lamellae of collagen fibrils bound with glycosaminoglycans (GAGs) (23).

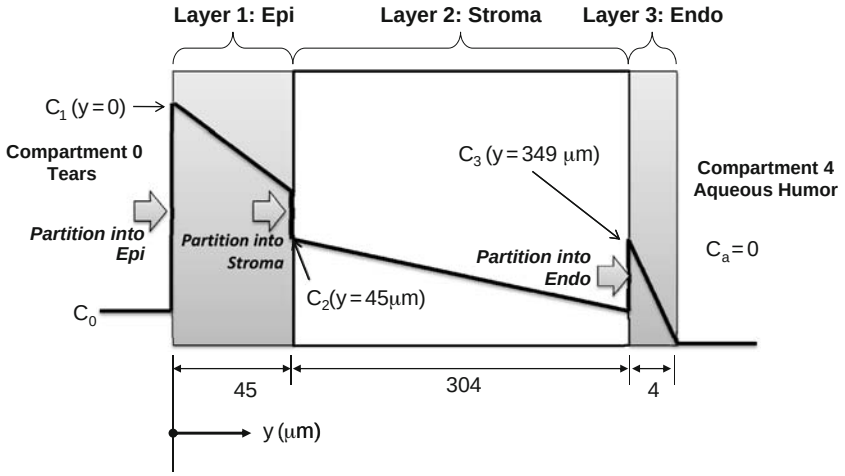

Fig. 4. Partition equilibrium of a lipophilic topical drug: Suppose C_0 is the concentration of the topical drug in the tears at an instant t. Then, partitioning of the drug into the epithelium results in a concentration C_1 (at y=0) at its outer boundary given by (PC × C_0), where PC is the partition coefficient between tears (equivalent to a buffer) and lipid-rich epithelial layer (equivalent to octanol). Once the drug is in the epithelium, it diffuses down along its concentration gradient in the epithelium. Abbreviations: C_1: Concentration in epithelium; C_2: Concentration in stroma; C_3: Concentration in endothelium; C_a: Concentration in the anterior chamber; y: Depth across cornea.

In general, a solute could bind to collagen and GAGs. We assume that binding-unbinding reactions occur at a faster time scale compared to that of diffusion. This assumption is consistent with the experimental data on diffusion of small molecules in artificial collagen networks, which suggests that the binding-unbinding events are rapid, and transport of small solutes is governed by diffusion alone (24). Therefore, the bound and unbound forms are always at equilibrium, so we need to address the mass balance for the total solute only. Accordingly, the following describes RhB transport across the stroma:

$$\frac{\partial C_2}{\partial t} = D_2 \frac{\partial^2 C_2}{\partial y^2} \tag{3}$$

where D_2 and C_2 are effective diffusivity and total concentration of the solute in the stroma, respectively (Table I).

Boundary Conditions

At the tear-epithelium interface, the solute concentration in epithelium is at equilibrium with concentration in tear fluid. This can be written as

$$C_1 = \Phi_{10} C_0 \tag{4}$$

where Φ_{10} is the partition coefficient between the epithelium and the tears and C_0 is the drug concentration in tears (Table I and Fig. 4). At the epithelium-stroma interface, we

Table I. Description of Model Parameters

Parameter	Units	Definition
Φ_{10}	–	Ratio of average concentration in epithelium bilayer (based on total cell volume) to concentration in tears at equilibrium
K_1	–	Ratio of average concentration in epithelial bilayers (based on total cell volume) to concentration in internal hydrophobic regions (based on total cell volume) at equilibrium
k_1	s^{-1}	Permeability of cytoplasmic medium separating lipid bilayers and internal hydrophobic regions in epithelium
D_1	m^2/s	Diffusion coefficient of RhB in lipid-bilayers in epithelium
k_{perm}	m/s	Permeability coefficient of epithelium-stroma interface
Φ_{21}	–	Ratio of concentration in stroma to average concentration in epithelium bilayers (based on total cell volume) at equilibrium
D_2	m^2/s	Diffusion coefficient of RhB in stroma
Φ_{32}	–	Ratio of average concentration in endothelium bilayers (based on total cell volume) to concentration in stroma at equilibrium
K_3	–	Ratio of average concentration in endothelium bilayers (based on total cell volume) to that in internal hydrophobic regions (based on total cell volume) at equilibrium
k_3	s^{-1}	Permeability of cytoplasmic medium separating lipid bilayers and internal hydrophobic regions in endothelium
D_3	m^2/s	Diffusion coefficient of RhB in lipid bilayers of endothelium

expect concentration equilibrium and flux continuity. We model the condition of concentration equilibrium as

$$D_1 \frac{\partial C_1}{\partial y} = k_{perm}\left(C_1 - \frac{C_2}{\Phi_{21}}\right) \quad (5)$$

where k_{perm} is the permeability of epithelium-stroma interface and Φ_{21} is the equilibrium partition coefficient between the stroma and the epithelium (Table I and Fig. 4). The partition coefficient Φ_{21} is the ratio of the concentrations in phase 2 (stroma) and phase 1 (epithelium) at equilibrium, and it can be represented as $\Phi_{21} = \frac{\Phi_{20}}{\Phi_{10}}$, where Φ_{20} and Φ_{10} are the partition coefficients of phases 2 and 1, respectively, with respect to tears. Inclusion of the permeability at the epithelium-stroma interface in Eq. 5 is consistent with the observed increasing concentration gradient with time in the epithelium and the development of concentration peak at the epithelium-stroma interface. In Eq. 5, $1/k_{perm}$ represents mass transfer resistance at the interface. When k_{perm} is large, Eq. 5 correctly reduces to the concentration equilibrium requirement. As discussed later, we have evaluated the model with and without the k_{perm} parameter. For flux continuity, we impose the following boundary condition at the interface:

$$D_1 \frac{\partial C_1}{\partial y} = D_2 \frac{\partial C_2}{\partial y} \quad (6)$$

We now specify similar boundary conditions for the interface between the stroma and endothelium, but we assume that the interface concentrations to be in equilibrium so that

$$\begin{aligned} D_2 \tfrac{\partial C_2}{\partial y} &= D_3 \tfrac{\partial C_3}{\partial y} \\ C_3 &= \Phi_{32} C_2 \end{aligned} \quad (7)$$

Finally, at the endothelium-aqueous humor interface, the diffusing drug is swept away rapidly from the interface, and thus a reasonable representation of this is to set the concentration to zero (i.e., sink conditions):

$$C_3 = 0 \quad (8)$$

The perfect sink condition in Eq. 8 is a reasonable assumption due to the high volume (~300 μL) of the receiver chamber and the rapid perfusion rate of ~3 μL/min. The initial conditions correspond to zero concentration across the entire cornea and the known initial concentration of the solute in the tears.

Parameter Estimation

We have employed unsteady state concentration profiles of RhB in Fig. 2 to estimate the 11 parameters (Table I) in the above model. We first note that the model has no non-linear terms so that the concentration at any point across the cornea would be proportional to the solute concentration in tears. Second, at the low concentration used, fluorescence of RhB is linearly proportional to concentration so that measured fluorescence value represents concentration of diffusing RhB. Therefore, we use the fluorescence and the solute concentration across the cornea interchangeably in the following estimation procedures.

Initial Guess for Parameter Estimation

For the case of constant concentration in the tears (C_0), the concentration at the tear-epithelium interface ($y=0$) can be given by

$$\begin{aligned} C_t(y=0) &= C_1(y=0) + C_1^b(y=0) \\ &= C_0\left(\Phi_{10}(1+K_1) - \Phi_{10}K_1 e^{-\frac{k_1}{K_1}t}\right) \end{aligned} \quad (9)$$

Since C_0 was constant in our measurements, a plot of experimental C_t ($y=0$) *vs.* t can be fitted to Eq. 9 for estimating Φ_{10}, K_1, and k_1. At t ~0 or smaller, at the epithelium-stroma interface, the ratio of the total concentration at the stroma to the epithelium is the partition coefficient Φ_{21}. The diffusivity of the solute in stroma (D_2) is assumed to be that in free solution, and the diffusivity in epithelium (D_1) is approximated by multiplying D_2 with the ratio of average slopes of concentration profiles in the stroma and epithelium. The value of D_3 is expected to be equal to D_1, recognizing that both consist of similar biological cell layer(s). Also, the values of k_3 and K_3 are expected to be equal to k_1 and K_1, respectively. With these initial constraints imposed on the parameters of Eqs. 1–9, we developed a MATLAB program that estimated model parameters by minimizing the sum of the residual errors (denoted by E) between the calculated and measured fluorescence (i.e., concentration) values.

The measured fluorescence at a given depth y arises from the excitation of all fluorophores at the neighborhood and is obtained by convoluting the concentration profiles with the instrument response function (IRF) given by

$$IRF(y - y') = \frac{e^{-\frac{(y-y')^2}{2\sigma^2}}}{\sqrt{2\pi\sigma^2}} \quad (10)$$

where (2.36 σ) represents full width of the Gaussian. This was measured to be ~10 μm for the 40x objective (Zeiss, 0.75 NA; water immersion) and a defined excitation and emission slit widths employed during the measurements (18,19,22). Further, since the measured fluorescence arises from RhB present both in the cellular bilayers as well as intracellular lipophilic domains, we write

$$C_{total} = C_i + C_i^b \quad (11)$$

where $C_i$and C_i^b represent concentrations in the cellular bilayers and intracellular lipophilic domains. Note C_i^b and C_3^b represent the bound RhB in the epithelium and endothelium, respectively.

To compare the model prediction (C_{Model}) with measured fluorescence values, we performed convolution of C_{total} with IRF as

$$C_{Model}(y') = \int_0^\infty C_{total}(y)\ IRF(y - y')dx \quad (12)$$

We define the following objective function for estimating the model parameters:

$$E = \sum_{i=i}^{3} \sum_{k=1}^{N_i} \left[\left(C_{Model} - C_{Exp}\right)^2\right]_k \quad (13)$$

where C_{Exp} is the measured concentration at a given position and time t, N_i is the total number of data points in the i^{th}

layer, with i=1 – 3 (representing the three corneal layers), and C_{Model} is RhB concentration predicted by the model. The number of points in each layer N_i is the product of the total number of data points at each time step and the total number of time instants at which data were recorded. The error function (E) was minimized using the *fminsearch* program of the MATLAB to obtain optimal parameter values. The values of the parameters thus estimated are given in Table II, and the model predicted fluorescence profiles are compared with the experimental data in Fig. 5. We also examined cases with and without inclusion of the k_{perm} parameter (Eq. 5). The parameters given in Table II are only provided for the case with k_{perm}, since the profiles without this term did not match the data well, and in particular the model without k_{perm} cannot capture the characteristics (b) and (c) of the transient concentration profiles listed above.

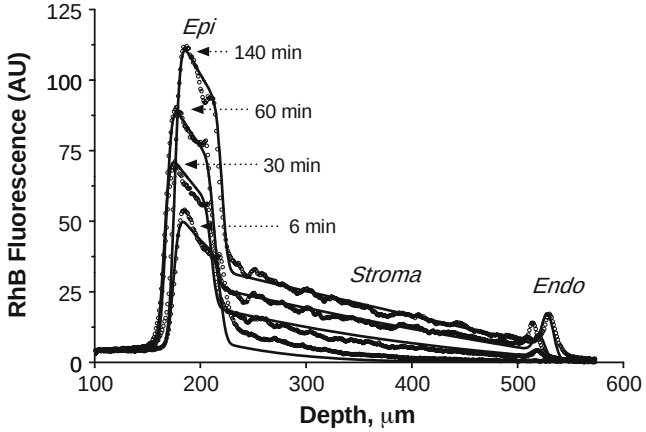

Fig. 5. Comparison of model predictions (solid lines) and experimental measurements (circles) for transient fluorescence profiles in cornea at t=6, 30, 60, and 140 min.

Parameter Sensitivity Analysis

In order to check for the robustness of the model, we examined the identifiability of parameters by constructing sensitivity contour plots and calculating parameter correlation coefficients (25). The sensitivity contour plots consisted of contour lines of E (i.e., iso-E lines; calculated using Eq. 13) for variations in parameters taken one pair at a time, keeping all other parameters at their estimated values. Thus, for any parameter pair to be uncorrelated and be true/robust estimates (i.e., based on global minimum of E), we expect that the E contours would show a single minima that would converge toward small circles or small line segments. Contours that manifest as long lines should imply that the optimal values of the parameters are not unique, i.e., different sets of parameters could yield the same minimum error, and thus the parameters are not identifiable. Specifically, long horizontal lines imply that the parameters on the x-axis are not identifiable, and, similarly, long vertical lines imply that the y-axis parameter is not identifiable. Long slanted lines imply that the parameters on the x and the y axes are correlated.

Table II. The Optimal Values of the Model Parameters Obtained by Minimizing the Total Error Between the Model Prediction and Experimental Data for RhB Concentration in Cornea at Various Times

Parameter	Estimated value	Units	Sensitivity index
Φ_{10}	9.8	–	*100.27*
K_1	1.6	–	*6.39*
k_1	4×10^{-4}	s^{-1}	*4.48*
D_1	7.9×10^{-12}	m^2/s	*3.01*
k_{perm}	6×10^{-8}	m/s	*10.36*
Φ_{21}	10.6	–	*0.11*
D_2	22.8×10^{-12}	m^2/s	*4.92*
Φ_{32}	2.8	–	*0.54*
k_3	3×10^{-4}	s^{-1}	*0.01*
K_3	1.2	–	*0.02*
D_3	1.5×10^{-12}	m^2/s	*0.78*

Sensitivity analysis of the transport model. Values of the sensitivity index larger than 5 indicate that error between the experimental data and the model fit increased by less than 5% for a 10% change in the model parameter and imply a robust fit and a reliable value of the fitted parameter.

In order to examine the kinetic model, contour plots for 55 possible pairs of parameters pairs ($^{11}C_2$ combinations) were constructed around the minima using MATLAB and defined by the parameter estimates in Table II (Col. 3). Each of the parameters was varied ±50% around the estimate. Illustrative cases of E contour plots are shown in Figs. 6 and 7. For Φ_{10} -D_2 and Φ_{10}-K_1 parameter pairs, the error contours are shown in Fig. 6A and C, respectively. The error minima converges along small, vertical line segments, which eventually converge to a point. These observations confirm, as expected, negligible correlation between Φ_{10} and D_2 as well as between Φ_{10} and K_1. Similarly, the limiting contours for k_1 -D_2 and D_1-k_{perm} pairs presented in Fig. 6B and D, respectively, represent small horizontal line segments converging to a point. Again, these plots indicate a negligible correlation between k_1 and D_2 as well as D_1 and k_{perm}. In contrast to these plots, which are representative of robust parameter estimates, we also found that certain estimates appear to be ill-identified. For example, E contours for the D_3-D_1 pair shown in Fig. 7A where two contours have same values of error. This implies that the parameter estimation might depend on the initial guesses of the parameters. However, the minima are relatively close to each other. Similarly, for the k_3-K_3 pair, the parameter estimation might depend on starting parameter values (Fig. 7B). The plots involving parameter Φ_{21} in Fig. 7C and D show that the y-axis parameter Φ_{21} is not well defined because the contour plots are vertical lines.

We have next quantified the information implied in contour plots above in terms of correlation coefficients between all the parameters of the model. The calculated values for the possible 55 combinations of parameter pairs are given in Table III. For the purposes of emphasizing the importance of E-contours vis-à-vis Table III, the coefficients for the parameter pairs employing-contours shown in Figs. 6 and 7 are highlighted (shaded and bold text). A parameter is well identified if its regression coefficient with all other parameters lies between $-0.9 < r < 0.9$ (25). As per this criterion, it is evident from Table III that most of the parameters are well identified, with the exception of Φ_{21}, Φ_{32}, and K_3. This conclusion is consistent with those drawn on the basis of the contour plots in Figs. 6 and 7.

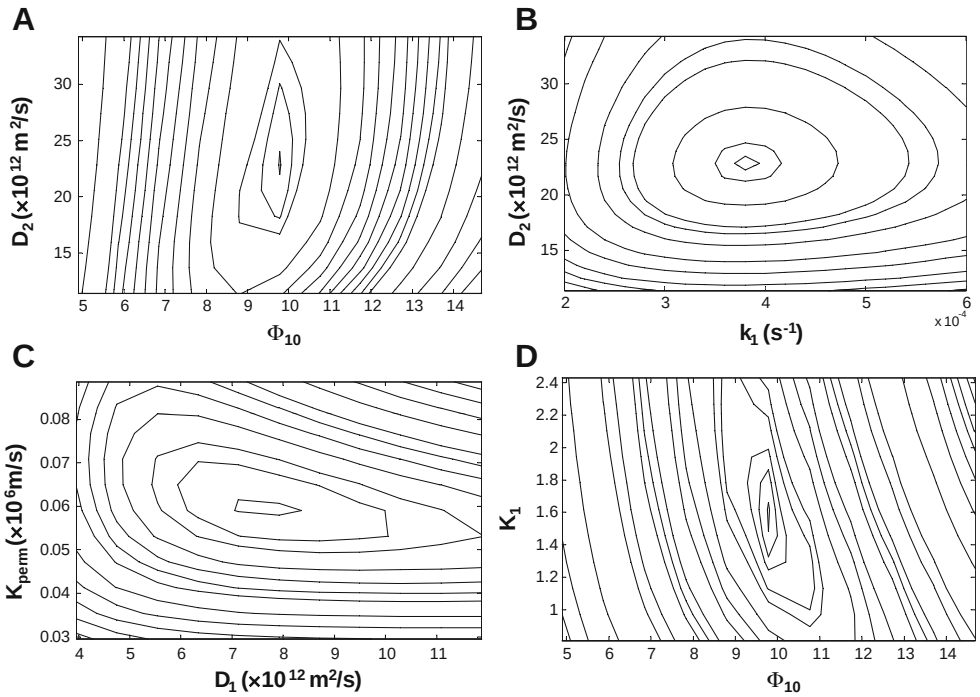

Fig. 6. Contour plots of error, i.e., square of the difference between the model predictions and experimental values for Rhodamine B concentration in cornea (Eq. 13). The parameters on the x and the y axes are varied in a range of ±50% around the optimal values, while keeping all other variables fixed at the optimal values. The contours in each case show a single minimum and contours converge, proving that the fitting is robust and the pair of parameters [Φ_{10}-D_2 in (a); k_1 -D_2 in (b) Φ_{10}-K_1 in (c) K_{perm}-D_1 in (d)] are uncorrelated [a-d are clockwise starting from top left].

Single Parameter Sensitivity Analysis

We next determined the sensitivity of each parameter vis-à-vis total error E defined by Eq. 13. Since all parameters except one are fixed in this calculation, the error function is expanded as a Taylor series at the point of minimum error,

$$E = E_{min} + \frac{1}{2}\frac{d^2E}{du^2}\bigg|_{u_{min}} (u - u_{min})^2 \qquad (14)$$

where E_{min} is the minimum error or the error corresponding to the optimum parameter. The parameter u in the above denotes any one of the eleven model parameters. u_{min} is the value of u at which the error is minimum. In Eq. 14, the linear term is absent, as the first derivative (dE/du) is zero at the minimum. We further define a dimensionless sensitivity parameter α derived from Eq. 14:

$$\alpha = \frac{\left[\frac{E-E_{min}}{E_{min}}\right]}{\left[\frac{u-u_{min}}{u_{min}}\right]^2} \equiv \frac{{u_{min}}^2}{2E_{min}}\frac{d^2E}{du^2}\bigg|_{u_{min}} \qquad (15)$$

where the index α quantifies the changes in E due to changes in u. For instance, a value of 5 for α implies that 10% change in the parameter from its optimal estimate (i.e., $u\text{-}u_{min}=0.1\ u_{min}$) gives a 5% change in error ($E\text{-}E_{min}$). To calculate α for a specific value of u, we determined the second derivative in Eq. 15 computing E around u_{min} and then fitting the resulting data to a quadratic polynomial. The calculated values of α shown in Table II indicate that Φ_{21} and the parameters involving endothelium (i.e., Φ_{32}, K_3, k_3, and D_3,) are << 5, suggesting that the model is insensitive to these parameters, which indicates that they may be poorly identified. This is consistent with the conclusions drawn from the contour plots (Figs. 6 and 7) and the correlation matrix (Table III). The lack of sensitivity of the parameters involving endothelium could be attributed to limited sampling of RhB in the monolayer given its smaller thickness compared to other layers; the sampling interval was 0.5 μm. The lack of sensitivity to Φ_{21} occurs because the transport from the epithelium to the stroma is limited by the barrier offered by the epithelium-stroma interface, so small changes in the stromal concentration have a negligible impact on the flux at the epithelium-stroma interface.

Modeling *In Vivo* Kinetics

Guss *et al.* (17) instilled a drop of 0.1% RhB on the surface of the cornea of rabbits and measured the concentration transients in the epithelium, stroma, and aqueous humor. However, the study did not report the concentration profiles across each of the layers due to a lack of high-depth resolution in their measurements. Therefore, the measured values represent spatial averages in different layers. The model described in Eqs. 1–10 can be employed to predict the *in vivo* pharmacokinetics with the caveat that RhB concentration in tears decreases exponentially after administration

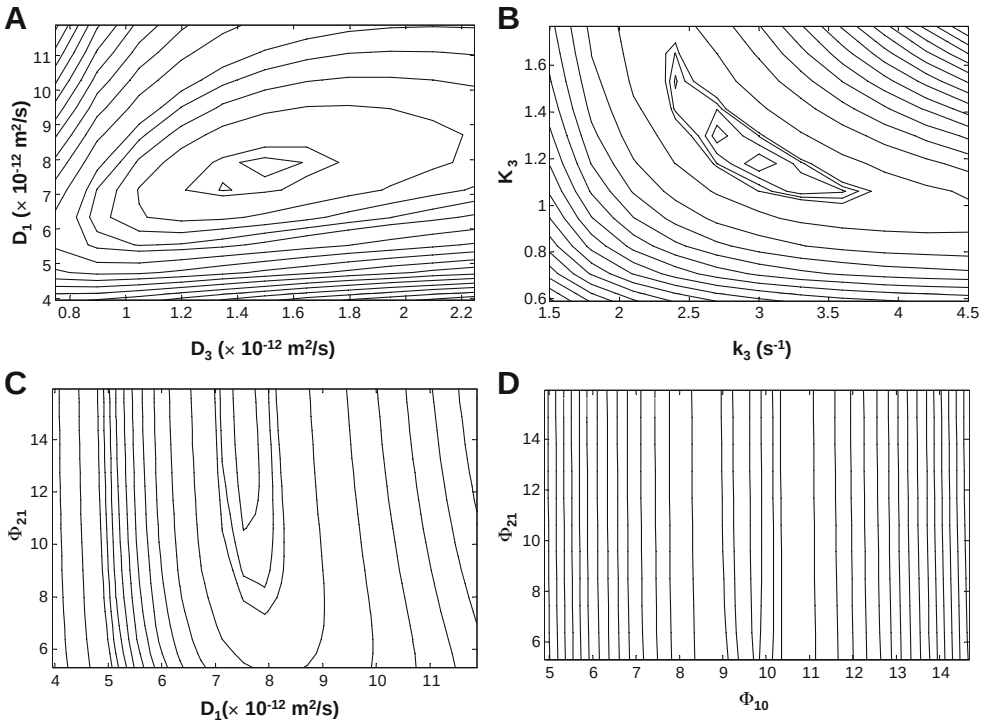

Fig. 7. Contour plots of error, i.e., square of the difference between the model predictions and experimental values for Rhodamine B concentration in cornea (Eq. 13). The parameters on the x and the y axes are varied in a range of ±50% around the optimal values, while keeping all other variables fixed at the optimal values. The contour plots in Panels A and B show closely spaced multiple minima, implying that the value of the optimal parameters predicted by the error minimization (D_3-D_1 in Panel A) and k_3-K_3 in Panel B) would vary slightly depending on the initial guess of the parameters. The contours in Panels C and Panel D are straight lines, proving that variation of Φ_{21} has a negligible effect on error if $\Phi_{21}>10$.

of a drop (7). Therefore, we assume tear RhB concentration as

$$C_{tear} = C_0\, e^{\frac{-t}{\tau}} \tag{16}$$

where C_0 is the initial concentration of RhB (after accounting for dilution in the tears) and τ is the time constant of elimination from the corneal surface. This modifies the boundary condition at $y=0$ as

$$C_1 = \Phi_{10}\, C_{tear} = \Phi_{10}\, C_0\, e^{-\frac{t}{\tau}} \tag{17}$$

Additionally, we incorporate the anterior chamber dynamics into the *in vitro* model to account for RhB clearance *in vivo*, which occurs largely through aqueous humor outflow. Thus, the mass balance in the anterior chamber can be given by

$$V_{aq}\frac{\partial C_{aq}}{\partial t} = -D_3 A_{cornea}\frac{\partial C_3}{\partial y} - K_{clearance}\, C_{aq} \tag{18}$$

where C_{aq} is the concentration of RhB in the anterior chamber (which is assumed to be well-mixed), V_{aq} is the

Table III. Coefficient of Correlation Between All the Model Parameters Obtained by Fixing All Parameters Except the Two Chosen Parameters

	Φ_{10}	K_1	k_1	D_1	k_{perm}	Φ_{21}	D_2	Φ_{32}	K_3	k_3	D_3
Φ_{10}	1	-0.13	-0.32	-0.42	-0.05	–	0.06	0.12	-0.2	-0.33	0.22
K_1		1	-0.53	-0.14	0.12	-0.32	0.12	0.04	0.35	0.34	0.01
k_1			1	-0.54	-0.02	*0.91*	-0.09	-0.25	0.61	0.35	-0.08
D_1				1	-0.19	–	0.55	*0.82*	0.01	-0.14	-0.19
k_{perm}					1	-0.19	0.61	0.16	0.11	0.03	0.19
Φ_{21}						1	0.03	0.60	-0.15	-0.16	-0.03
D_2							1	-0.28	*0.98*	0.03	-0.2
Φ_{32}								1	0.30	0.31	*-0.90*
K_3									1	-0.1	0.71
k_3										1	*0.81*
D_3											1

Correlation coefficient is calculated for the limiting contours encompassing the minima. Coefficient of correlation should lie between -0.9 and 0.9 for variables to be uncorrelated. High values of correlation coefficients have been italized in the table. The blank entries in the table correspond to the cases of vertical or horizontal contours for which the correlation coefficient is undefined, ex., contour plots in Fig. 7 (c-d).

volume of anterior chamber, $K_{clearance}$ is the total clearance from anterior chamber, and A_{cornea} is the surface area of cornea. The values of V_{aq} and A_{cornea} for rabbits were assumed to be 0.311 mL and 1.54 cm^2, respectively (26). $K_{clearance}$ is approximated as the aqueous humor outflow in rabbits, which is reported to vary from 0.411 μL/min (27) to about 3 μL/min (28,29). A value of 0.411 μL/min was used in the simulations reported here, but higher values would result in similar predictions for corneal concentrations as the aqueous humor concentrations are close to perfect sink (i.e., close to zero concentration). Drop volume is assumed to be 30 μL (21). The value of τ was taken to be 1 min because the tear concentration drops to negligible values a few minutes after instillation (1,4,7,21,30). Based on these considerations, we computed the concentration transients for spatially averaged concentration in epithelium. The comparison of the predicted values to those reported by Guss *et al.* (17) is presented in Fig. 8. The comparison is not exact but is comparable, despite the variability in the physiological parameters and the uncertainty in the tear concentrations. The value of $K_{clearance}$ is also uncertain because of binding to various tissues and diffusion through the lens (shown significant RhB accumulation in lens (17)); however, its uncertainty has very little impact on the concentration transients in epithelium as the concentration in anterior chamber is sufficiently close to perfect sink conditions for most of the time.

DISCUSSION

In this study, we established a kinetic model for characterizing transport of a lipophilic solute across the cornea. Most models on the trans-corneal penetration kinetics reported to date are based on the method of compartmental modeling (10-12). A few studies that attempted to characterize the diffusive transport across each of the corneal layers lacked experimental evidence of trans-corneal concentration profiles (14-16). The model developed in this study accounts not only for the multi-laminate structure of the cornea (Fig. 1) but also is based on temporal and spatial experimental concentration profile of a fluorescent dye, RhB, as a lipophilic drug analog. Because of corneal transparency, we measured unsteady state trans-corneal profiles of RhB. These novel data provide experimental evidence for a mechanistic description of the trans-corneal transport, and as a result enabled development of a physiology-based pharmacokinetic model. It is worthy to note that the fluorescent dye RhB has been previously used as a model drug surrogate for characterizing transport across the skin (31,32), cornea/lens (17,33), and conjunctiva/sclera (34).

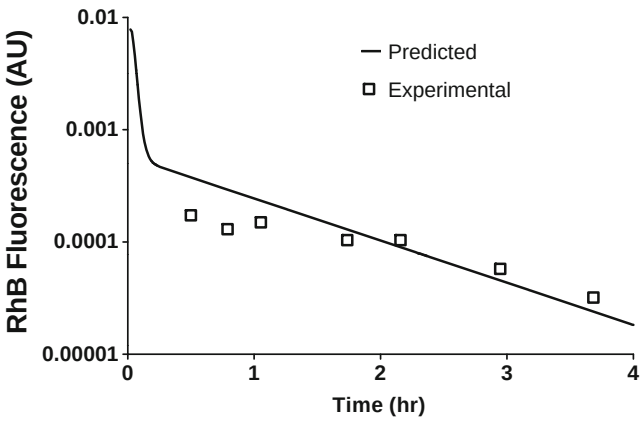

Fig. 8. Comparison of experimental data by Guss *et al.* (17) and model prediction for spatially averaged transient epithelium concentration of RhB in rabbit cornea. In the experiment by Guss *et al.*, a single drop of 1% RhB was instilled in the rabbit eye.

Modeling Interphase and Intraphase Transport

A novel aspect of our model is the integration of the multi-laminate view of the cornea illustrated in Fig. 1. Although this model is well known (1,4,5,35), models for topical pharmacokinetics, in general, have failed to include the existence of heterogeneous nature (i.e., presence of three distinct phases) across the cornea. RhB, being a lipophilic molecule (octanol-water partition coefficient: 100–310) (17,32), turned out to be very useful in mimicking a lipophilic drug analog. Its trans-corneal distribution not only highlights interphase transport (i.e., lipophilic layer →hydrophilic layer →lipophilic layer) but also demonstrated a unique mechanism of intra-phase transport within the cellular layers, namely the epithelium and endothelium. To accommodate inter-phase transport, we formulated partitioning at the interface (Eqs. 4, 5, and 7) and also modeled interfacial resistance (Eq. 5) for transport across the epithelium-stroma interface. For describing intra-phase transport in the stroma, we assumed homogeneous transport properties, but the solute transport is by diffusion (Eq. 3). For transport across the cellular layers, we incorporated an additional length scale in describing the diffusive transport. In this approach, the transport is modeled as diffusion across the bilayers of plasma membrane and partitioning into intracellular lipophilic domains. Since the concentration in the cytoplasm is expected to be small for lipophilic solutes, partitioning into such domains is likely to be prolonged (as discussed previously in the model section). We believe that the slow accumulation of RhB in the cellular layers (Fig. 2) and a continuous increase in the observed RhB fluorescence at the tear-epithelium interface shown in Fig. 2 support our reasoning. Therefore, we conclude that the transport of lipophillic molecules across the cellular layers is rate limited by transport across the hydrophilic cytoplasm. It is again noted that slow binding of RhB to binding sites inside the cells could also lead to slow accumulation evident in the experimental data, and further experiments are needed to conclusively determine the correct mechanism for the slow accumulation.

Model Validation

In terms of model validation, uncertainties in the model from the point of view of estimated parameters have been analyzed extensively. However, model verification with multiple fluorescent dyes was beyond the scope of the current study and need to be considered in further studies. As a first step in the success of our model, we note that the parameters in Table II predicted the experimental data accurately. Second, the calculated parameters exhibited high sensitivity, and the estimated values were independent of starting initial estimate. This conclusion is based on the sensitivity analysis

presented in error (E) contour plots (Figs. 6 and 7) and the correlation coefficients between the parameters (Table III). As noted earlier, three of the parameters, namely Φ_{21}, Φ_{32}, and k_3, showed poor sensitivities, indicating a need for additional experiments to accurately determine their values. As noted earlier, it is possible that this can be overcome by overcoming the inadequate sampling across the endothelium given its small thickness (4 μm) (36).

A principal set of parameters relating to transport and phase equilibrium at tear-epithelium, epithelium-stroma, and stroma-endothelium interphase are given in Table I. To establish the validity of these parameters, it is instructive to compare the values reported in Table I with values previously reported in literature. The parameters K_1 and K_3 have never been measured or estimated previously, so we cannot compare our fitted values to any prior measurements. The parameter $1/k_1$, the time constant of transfer of drug from lipid bilayer to other hydrophobic domains in epithelium, has not been reported, and thus a direct comparison with measurements is not feasible. A scaling analysis shows that this parameter is about $5\,\Phi_{10}\,R^2/D_{1C}$, where R is the radius of the epithelial cell and D_{1C} is the diffusivity of RhB in the cytoplasm of the epithelial cells. Setting R=8.3 μm, $D_{1C}=4\times10^{-12}$ m^2/s (based on Stokes Einstein equation (37)) and Φ_{10}=10, we get $1/k_1$=800 s, which is significantly lower than the fitted value of 2,500 s (Table II). Nonetheless, the value obtained from the scaling analysis is of the same order of magnitude as the fitted value, which is encouraging, particularly considering the assumptions implicit in the scaling analysis and the uncertainty in the values of the parameters utilized in the scaling calculations. The reasonable agreement between the fitted values and those obtained from the scaling analysis supports the assertion that the slow accumulation of RhB is the cornea is due to transport across the cytoplasm into internal organelles. However, single-cell studies are required to conclusively prove this hypothesis.

The time constant of transfer of drug from lipid bilayer to other hydrophobic domains in endothelium is about $5\Phi_{30}\,R^2/D_{3C}$, which should be approximately equal to the value obtained for the epithelium, i.e., 800 s, due to similarities in the structure of the epithelium and endothelium cells. This value is in reasonable agreement with the fitted value of 3,330 s (Table II). Based on a model reported by Zhang *et al.*, the diffusivity of a 0.55 nm size lipophillic molecule in epithelium should be $\sim2\times10^{-12}$ m^2/s. Our fitted value of 7.9×10^{-12} m^2/s is in reasonable agreement with the value predicted by the model. Similarly, based on Zhang *et al.* (16), the diffusivity in endothelium should be $\sim2\times10^{-12}$ m^2/s, which is in good agreement with the fitted value of 1.5×10^{-12} m^2/s. Zhang *et al.* (16) also reported a value of diffusivity in stroma as 2.2×10^{-10} m^2/s, which is an order of magnitude higher than the fitted value of 2.3×10^{-11} m^2/s. The discrepancy between the value estimated from the model of Zhang *et al.* (16) and that obtained by fitting the transient profiles is likely due to significant binding of the drug in stroma to collagen and proteoglycans.

The value of the partition coefficient between the stroma and tears $\Phi_{20}=\Phi_{21}\times\Phi_{10}$ is ~100, which is much larger than 1, even though stroma is almost water-like, supporting the hypothesis that a large fraction of RhB in stroma is bound. The bound and the free concentrations in the stroma are likely in equilibrium due to fast binding-unbinding kinetics, but the bound fraction does not diffuse, leading to a reduction in the value of the diffusivity by the ratio of the free drug to the total drug present locally (38). To our knowledge, there is no reported value of the barrier at the epithelium-stroma interface, and so a direct comparison with experiments is not feasible. The experimental profiles for fluorescence show a slight shoulder/peak at the interface between the epithelium and stroma, which appears to support the hypothesis that a thin layer at this interface presents a barrier to transport. Alternatively, the resistance could be due to an additional transport step of RhB from inside the lipid bilayers of the epithelium to the stroma. Further investigations are needed to examine this issue.

Asymptotic Behavior

In order to obtain further insights on the penetration kinetics, we examined the pseudo-steady-state behavior after a prolonged time after topical instillation. For this purpose, we have the time derivatives in the model to zero and then calculated concentration profiles. Under these conditions, the concentration in each layer is linear so that the transport across the cornea can be modeled by a lumped model with an overall permeability coefficient given by

$$K_{eff}=\frac{1}{\frac{L_{stroma}}{\Phi_{21}\Phi_{10}D_2}+\frac{L_{epi}}{\Phi_{10}D_1}+\frac{1}{\Phi_{10}k_{perm}}+\frac{L_{endo}}{D_3\Phi_{32}\Phi_{21}\Phi_{10}}} \tag{19}$$

where L_{epi}, L_{stroma}, and L_{endo} are the thicknesses of epithelium, stroma, and endothelium, respectively. To determine the time after which this lumped model can be employed, we calculated the diffusive time scales of each layer (L^2/D) and also for transport into the interior lipophilic domains given by $1/k_1$ and $1/k_3$. These characteristic times for the estimated parameters (Table II) are given in Table IV. The time required to reach pseudo-steady state was found to be ~60 min. This implies that for t<60 min, the lumped model is unsuitable for assessing the trans-corneal penetration. In

Table IV. Characteristic Time Scales for the Principal Mechanisms Included in the Model

Mechanism	Time scale	Time (min)
Diffusion in epithelium	$(L_{epithelium})^2 / D_1$	4.3
Diffusion in stroma	$(L_{stroma})^2 / D_2$	68.2
Diffusion in endothelium	$(L_{endothelium})^2 / D_3$	2.2
Transport from bilayers of plasma membrane into intracellular lipophilic domain in epithelium	$1 / k_1$	41.6
Transport from bilayers of plasma membrane into intracellular lipophilic domain in endothelium	$1 / k_3$	55.6

other words, for time up to 60 min, the unsteady terms in the mass balances must be included. Since the residence time of topical drugs is only a few minutes, it is clear that the lumped model is a poor representation of clinically relevant pharmacokinetics. However, the lumped model could be employed for describing transport *in vitro* experiments with diffusion chambers, as the topical concentration can be maintained constant over an extended time period.

Additional insights into trans-corneal transport can be obtained by comparing the transport resistance of each layer. Thus, using the estimated parameters, the transport resistance of stroma, epithelium, and endothelium and the interfacial resistance at the epithelium-stroma interface, respectively, are

$$\frac{L_{stroma}}{\Phi_{21}\Phi_{10}D_2} = 0.128 \times 10^6 s/m$$

$$\frac{L_{epi}}{\Phi_{10}D_1} = 0.58 \times 10^6 s/m$$

$$\frac{L_{endo}}{D_3\Phi_{32}\Phi_{21}\Phi_{10}} = 0.03 \times 10^6 s/m$$

$$\frac{1}{\Phi_{10}k_{perm}} = 1.73 \times 10^6 s/m$$

We note that that each layer, with the exception of the endothelium, offers significant resistance. The effective permeability of the cornea to RhB, based on Eq. 19, is 0.41×10^{-6} m/s, in reasonable agreement with permeability values reported in the literature for molecules with similar size and hydrophobicity (13). However, it should be emphasized that the overall permeability coefficient is not relevant for predicting pharmacokinetics of drugs delivered through eye drops because the residence time of drug is far less than the time required for reaching pseudo-steady state.

CONCLUSIONS

The mathematical model developed here accurately characterizes the transient solute transport through the cornea. The fitted values are reliable with a low level of uncertainty for all parameters except the endothelium parameters and the partition coefficient Φ_{21}. The model can predict the *in vivo* pharmacokinetics of RhB with reasonable accuracy. The model developed here is a significant improvement over conventional approaches using a lumped permeability approach because the drug residence time is much smaller than the time needed for establishing pseudo-steady. Thus, the lumped overall permeability is not a useful measure of total transport resistance.

ACKNOWLEDGEMENTS

Supported by NIH grant R21-EY019119 and Faculty Research Grant, VP of Research, IU Bloomington, IN (SPS).

REFERENCES

1. Maurice DM, Mishima S, editors. Ocular pharmacokinetics. Berlin: Springer-Verlag; 1984. p. 19–116.
2. Bourlais CL, Acar L, Zia H, Sado PA, Needham T, Leverge R. Ophthalmic drug delivery systems–recent advances. Prog Retin Eye Res. 1998;17:33–58.
3. Urtti A. Challenges and obstacles of ocular pharmacokinetics and drug delivery. Adv Drug Deliv Rev. 2006;58:1131–5.
4. Maurice DM. Prolonged-action drops. Int Ophthalmol Clin. 1993;33:81–91.
5. Gaudana R, Jwala J, Boddu SH, Mitra AK. Recent perspectives in ocular drug delivery. Pharm Res. 2009;26:1197–216.
6. Srinivas SP. *In situ* measurement of fluorescein release by collagen shields in human eyes. Curr Eye Res. 1994;13:281–8.
7. Wilson CG. Topical drug delivery in the eye. Exp Eye Res. 2004;78:737–43.
8. Wang Y, Chen M, Wolosin JM. ZO-1 in corneal epithelium; stratal distribution and synthesis induction by outer cell removal. Exp Eye Res. 1993;57:283–92.
9. Araie M, Maurice D. The rate of diffusion of fluorophores through the corneal epithelium and stroma. Exp Eye Res. 1987;44:73–87.
10. McLaren JW, Ziai N, Brubaker RF. A simple three-compartment model of anterior segment kinetics. Exp Eye Res. 1993;56:355–66.
11. Amrite AC, Edelhauser HF, Kompella UB. Modeling of corneal and retinal pharmacokinetics after periocular drug administration. Invest Ophthalmol Vis Sci. 2008;49:320–32.
12. Friedrich SW, Cheng YL, Saville BA. Theoretical corneal permeation model for ionizable drugs. J Ocul Pharmacol. 1993;9:229–49.
13. Ranta VP, Laavola M, Toropainen E, Vellonen KS, Talvitie A, Urtti A. Ocular pharmacokinetic modeling using corneal absorption and desorption rates from *in vitro* permeation experiments with cultured corneal epithelial cells. Pharm Res. 2003;20:1409–16.
14. Avtar R, Tandon D. Modeling the drug transport in the anterior segment of the eye. Eur J Pharm Sci. 2008;35:175–82.
15. Yamamura K, Sasaki H, Nakashima M, *et al*. Characterization of ocular pharmacokinetics of beta-blockers using a diffusion model after instillation. Pharm Res. 1999;16:1596–601.
16. Zhang W, Prausnitz MR, Edwards A. Model of transient drug diffusion across cornea. J Control Release. 2004;99:241–58.
17. Guss R, Johnson F, Maurice D. Rhodamine B as a test molecule in intraocular dynamics. Invest Ophthalmol Vis Sci. 1984;25:758–62.
18. Srinivas SP, Maurice DM. A microfluorometer for measuring diffusion of fluorophores across the cornea. IEEE Trans Biomed Eng. 1992;39:1283–91.
19. Maurice DM, Srinivas SP. Fluorometric measurement of light absorption by the rabbit cornea. Exp Eye Res. 1994;58:409–13.
20. Doughty MJ, Maurice D. Bicarbonate sensitivity of rabbit corneal endothelium fluid pump *in vitro*. Invest Ophthalmol Vis Sci. 1988;29:216–23.
21. Maurice DM, Srinivas SP. Use of fluorometry in assessing the efficacy of a cation-sensitive gel as an ophthalmic vehicle: comparison with scintigraphy. J Pharm Sci. 1992;81:615–9.
22. Srinivas SP, Maurice DM. Transport of rhodamine B across rabbit cornea. *Invest Ophthalmol Vis Sci Suppl*; 1991:1295.
23. Komai Y, Ushiki T. The three-dimensional organization of collagen fibrils in the human cornea and sclera. Invest Ophthalmol Vis Sci. 1991;32:2244–58.
24. Wallace DG, Rosenblatt J. Collagen gel systems for sustained delivery and tissue engineering. Adv Drug Deliv Rev. 2003;55:1631–49.
25. Beck JV, Arnold KJ. Parameter Estimation in Engineering and Science. New York: Wiley; 1977.
26. Mitra AK (ed) *Ophthalmic drug delivery systems*: Marcel Dekker, Inc.; 2003.
27. Tsonis PA. *Animal models in Eye Research*: Academic Press; 2008.
28. Reitsamer HA, Bogner B, Tockner B, Kiel JW. Effects of dorzolamide on choroidal blood flow, ciliary blood flow, and aqueous production in rabbits. Invest Ophthalmol Vis Sci. 2009;50:2301–7.
29. Reitsamer HA, Kiel JW. Relationship between ciliary blood flow and aqueous production in rabbits. Invest Ophthalmol Vis Sci. 2003;44:3967–71.
30. Maurice DM. Factors influencing the penetration of topically applied drugs. Int Ophthalmol Clin. 1980;20:21–32.
31. Yu B, Hean Kim K, So PT, Blankschtein D, Langer R. Topographic heterogeneity in transdermal transport revealed by high-speed two-photon microscopy: determination of representative skin sample sizes. J Invest Dermatol. 2002;118:1085–8.

32. Yu B, Dong CY, So PT, Blankschtein D, Langer R. *In vitro* visualization and quantification of oleic acid induced changes in transdermal transport using two-photon fluorescence microscopy. J Invest Dermatol. 2001;117:16–25.
33. Toropainen E, Ranta VP, Talvitie A, Suhonen P, Urtti A. Culture model of human corneal epithelium for prediction of ocular drug absorption. Invest Ophthalmol Vis Sci. 2001;42:2942–8.
34. Schoenwald RD, Deshpande GS, Rethwisch DG, Barfknecht CF. Penetration into the anterior chamber via the conjunctival/scleral pathway. J Ocul Pharmacol Ther. 1997;13:41–59.
35. Prausnitz MR, Noonan JS. Permeability of cornea, sclera, and conjunctiva: a literature analysis for drug delivery to the eye. J Pharm Sci. 1998;87:1479–88.
36. Srinivas SP, Bonanno JA, Lariviere E, Jans D, Van Driessche W. Measurement of rapid changes in cell volume by forward light scattering. Pflugers Arch. 2003;447:97–108.
37. Bird RB, Stewart WE, Lightfoot EN. *Transport Phenomena*: John Wiley & Sons, Inc.; 2002.
38. Kim J, Chauhan A. Dexamethasone transport and ocular delivery from poly(hydroxyethyl methacrylate) gels. Int J Pharm. 2008;353:205–22.